Supporting Information

High performance optical oxygen sensors based on nanostructured films incorporating bichromophoric iridium complexes exhibiting interchromophore energy shuttling

Santiago Medina-Rodriguez,[a] Sergey A. Denisov,[b] Yanouk Cudré,[c] Louise Male,[c] Marta Marin-Suarez,[a] Alberto Fernández-Gutiérrez,[a] Jorge Fernando Fernández-Sánchez,[a]* Arnaud Tron,[b] Gediminas Jonusauskas,[c] Nathan D. McClenaghan[b]* and Etienne Baranoff[d]*

[a] Department of Analytical Chemistry, Faculty of Sciences, University of Granada, Avenida Fuentenueva s/n, 18071 Granada, Spain

[b] Université Bordeaux/CNRS, ISM, 351 cours de la Libération, 33405 Talence Cedex, France

[c] Université Bordeaux/CNRS, LOMA, 351 cours de la Libération, 33405 Talence Cedex, France

[d] School of Chemistry, University of Birmingham, Edgbaston B15 2TT, United Kingdom

Content

I. Synthesis

General considerations. All the starting materials and solvents were commercially available and used as received. Solvents and acids were received from Fisher except for diethyl ether (Sigma-Aldrich) and 2-ethoxyethanol (Acros Organics). Silica gel (60, 0.040-0.063 mm, 230-400 mesh) was received from Alfa Aesar; 2-bromopyridine (99%) from Aldrich; tetrabutylammonium hydroxide (TBAOH·30 H_2O) from Sigma-Aldrich; 1-naphthaleneboronic acid and tetrakis(triphenylphosphine)palladium(0) from Acros Organics; 2,2,6,6-tetramethyl-3,5-heptanedione, boron trifluoride diethyl etherate and potassium hexafluorophosphate from Alfa Aesar; IrCl3·*x* H_2O from Heraeus. The complexes $Ir(npy)_2(MeCN)_2(PF_6)$, $Ir(npy)_2(tBubpy)(PF_6)$ (**Ir0**) and $Ir(npy)_2(bpy\text{-}pyr)(PF_6)$ (**Ir1**)[1] and the ligand 4,4'-bis(2-(pyren-1-yl)ethyl)-2,2'-bipyridine (bpy-pyr2).[2] were prepared as previously reported. ^1H spectra were recorded using a Bruker AVIII 500. Chemical shifts (δ) are expressed in ppm and referenced to the $CHCl_3$ residual peak (7.26 ppm). Coupling constants (*J*) are expressed in hertz (Hz). Mass spectrometry experiments were performed by means of electrospray ionisation on a Synapt G2-S HDMS mass spectrometer (Waters LTD, Manchester, UK).

Synthesis of $Ir(npy)_2(bpy\text{-}pyr2)(PF_6)$ (Ir2). $Ir(npy)_2(MeCN)_2(PF_6)$ (0.100 g, 0.12 mmol) was dissolved in 20 mL of degassed CH_2Cl_2/MeOH (9:1). After further degassing, the 4-methyl-4'-(2-(pyren-1-yl)ethyl)-2,2'-bipyridine, **bpy-pyr2**, was added. The mixture was gently heated to reflux (40 °C) overnight under argon atmosphere. The solvent was evaporated to dryness and the crude powder was dissolved in 30 mL of acetonitrile. A saturated aqueous solution of KPF_6 (50 mL) was added and the mixture was stirred at 40 °C for one hour. The solvent was gently evaporated until a precipitate formed. The mixture was left in the fridge for two hours and the precipitate was filtered, washed with water and dried under vacuum. The solid was then dissolved in a minimum amount of CH_2Cl_2 and precipitated with diethyl ether to remove the remaining unreacted ligand. The suspension was left in the freezer for 30 minutes, filtered and washed with diethyl ether. The complex was further purified by column chromatography on silica gel. The column was prepared with pure CH_2Cl_2 and the complex was adsorbed on the silica using pure CH_2Cl_2 as eluent. The column was eluted first with CH_2Cl_2 to eliminate the fast migrating impurities and then the eluent was changed to CH_2Cl_2/acetonitrile (80:20, v/v). The complex was purified further with multiple columns using CH_2Cl_2/methanol (95:5, v/v) as eluent until satisfactory analysis was obtained. **Ir2** was isolated as an orange powder (95 mg, 0.07 mmol, 58%). ^{1}H NMR (500 MHz, CD_3CN) δ 8.55 (d, J = 8.5 Hz, 2H), 8.44 (d, J = 8.6 Hz, 2H), 8.16 (d, J = 7.6 Hz, 2H), 8.14 (dd, J = 7.7, 1.0 Hz, 2H), 8.05 – 7.89 (m, 14H), 7.68 (dd, J = 8.2, 1.1 Hz, 2H), 7.52 – 7.47 (m, 6H), 7.40 (d, J = 5.6 Hz, 2H), 7.33 (ddd, J = 8.0, 6.9, 0.9 Hz, 2H), 7.28 (d, J = 1.2 Hz, 2H), 7.22 (d, J = 8.2 Hz, 2H), 7.00 (ddd, J = 7.3, 5.9, 1.3 Hz, 2H), 6.91 (dd, J = 5.6, 1.6 Hz, 2H), 6.22 (d, J = 8.3 Hz, 2H), 3.56 (dt, J = 14.0, 7.1 Hz, 2H), 3.48 – 3.40 (m, 2H), 3.09 (dt, J = 13.7, 6.9 Hz, 2H), 3.00 (dt, J = 13.4, 7.7 Hz, 2H). HRMS *m/z*: calc: 1213.3821, found: 1213.3826. Anal. Calcd. for $C_{76}H_{52}F_6IrN_4P$: C 67.20, H 3.86, N 4.12; found: C 67.07, H 3.80, N 3.94.

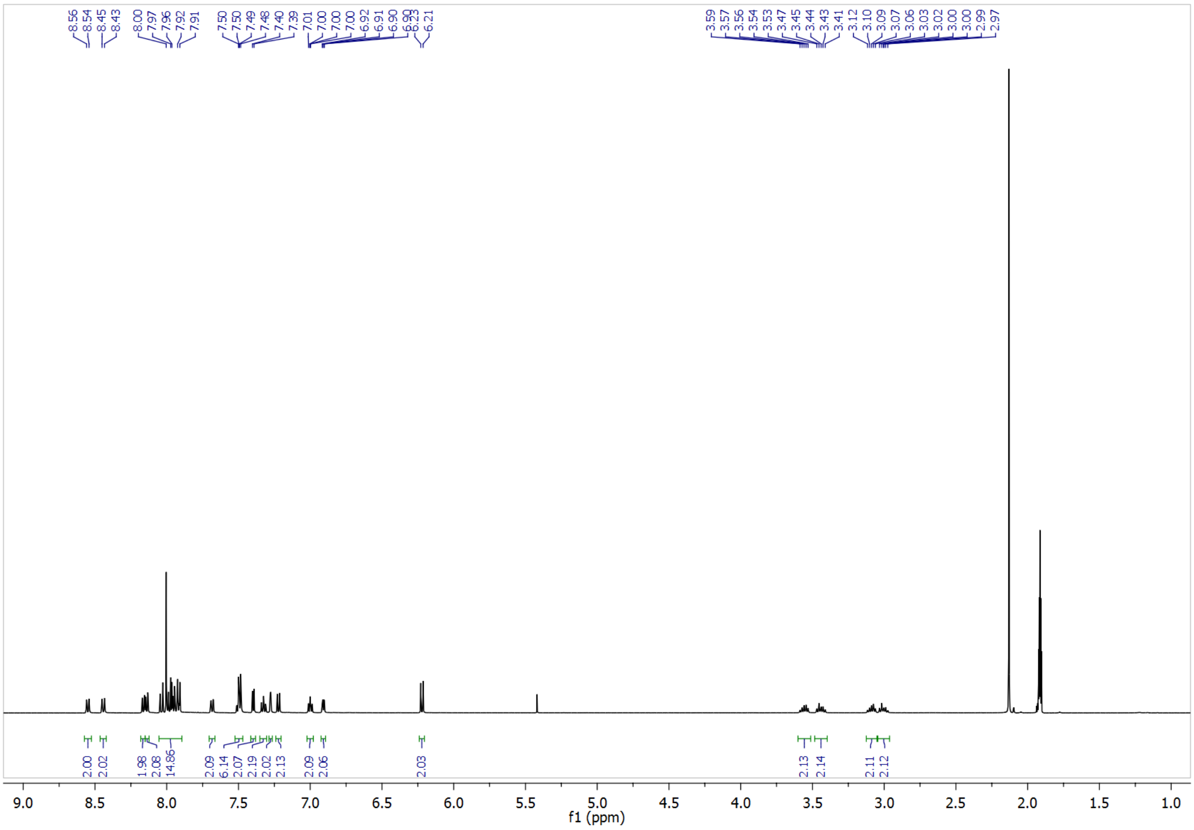

Figure S1. ^{1}H-NMR spectrum of **Ir2** measured in CD_3CN.

II. X-ray crystal structures

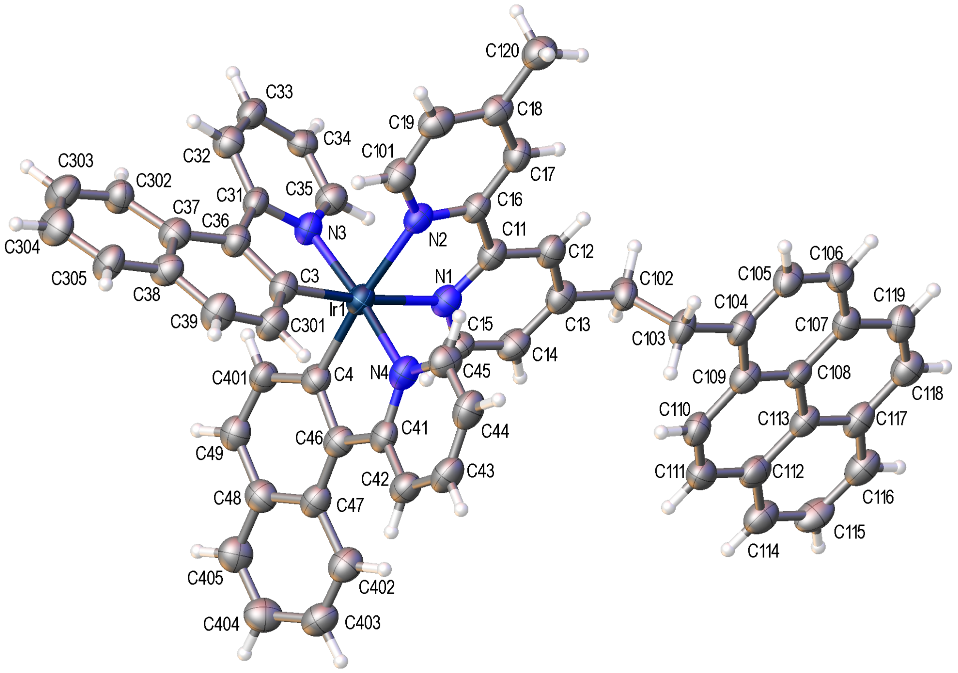

Figure S2. ORTEP drawings of **Ir1**.

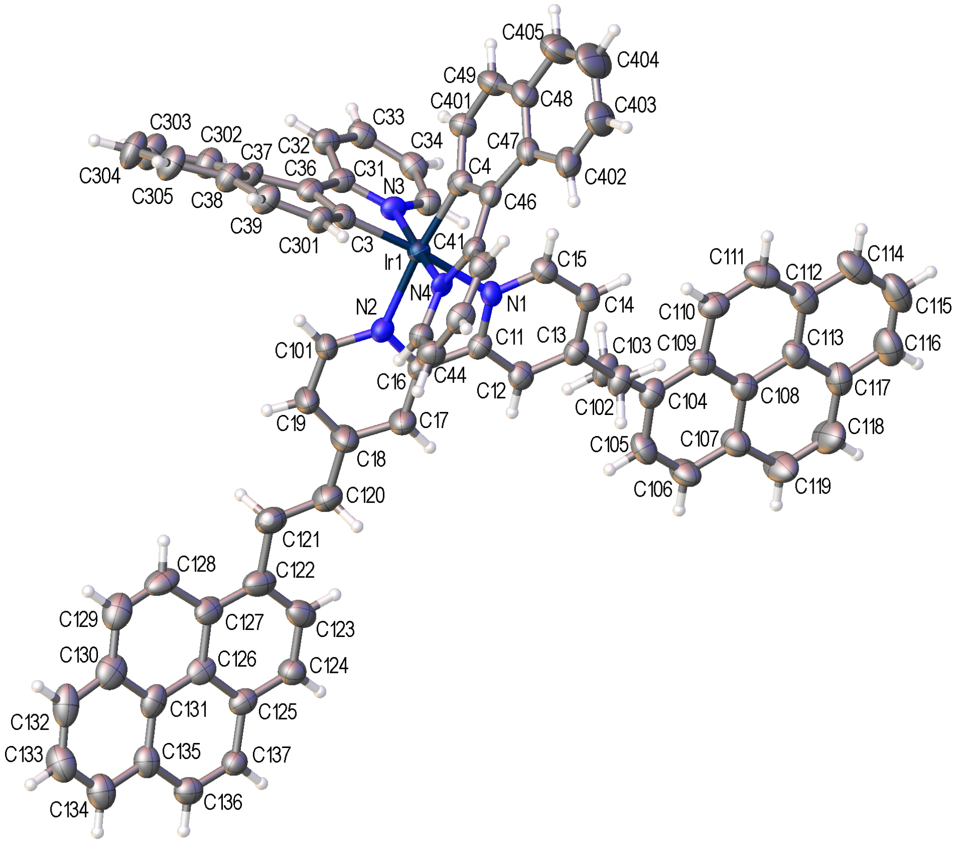

Figure S3. ORTEP drawings of one of the independent molecules of **Ir2**.

Table S1. Crystallographic data for **Ir1** and **Ir2**.

	Ir1•4 $CHCl_3$	**Ir2•1.25 CH_2Cl_2**
empirical formula	$C_{63}H_{46}Cl_{12}F_6IrN4P$	$C_{77.25}H_{54.5}Cl_{2.5}F_6IrN_4P$
formula weight	1621.61	1464.54
temperature, K	100.00(10)	100.00(10)
wavelength (Å)	0.71073	0.71073
crystal system	monoclinic	Triclinic
space group	$P2_1/c$	P-1
unit cell dimensions		
a (Å)	19.7764(14)	13.1487(9)
b (Å)	17.2133(11)	23.0231(16)
c (Å)	20.4799(14)	23.3516(16)
α (deg)	90	67.2098(19)
β (deg)	115.774(2)	75.538(2)
γ (deg)	90	78.319(2)
volume (Å^3)	6278.1(7)	6266.3(8)
Z	4	4
density, calc d (g/cm^3)	1.716	1.552
absorption coefficient (mm^{-1})	2.726	2.331
F(000)	3208.0	2938.0
crystal size (mm^3)	0.07 × 0.04 × 0.03	0.23 × 0.06 × 0.01
2θ range for data collection (deg)	6.076 to 51.36	5.91 to 51.362
reflections collected	37956	95074
independent reflections	11690 [R_{int} = 0.0850, R_{sigma} = 0.0622]	23701 [R_{int} = 0.1073, R_{sigma} = 0.0676]
data/restraints/parameters	11690/0/785	23701/70/1713
goodness-of-fit on F^2	1.041	1.027
final *R* indices [$I > 2\sigma(I)$]	R_1 = 0.0723 wR_2 = 0.1897	R_1 = 0.0673 wR_2 = 0.1815
R indices (all data)	R_1 = 0.0901 wR_2 = 0.2063	R_1 = 0.0807 wR_2 = 0.1939

III. Electrochemistry

Cyclic voltammetry (CV) measurements were performed on a PC controlled Autolab PGSTAT101 workstation. All experiments were realized using 0.1 M $TBAPF_6$ in acetonitrile as the electrolyte using three Pt electrodes as working, counter, and pseudo-reference electrodes. All solutions were degassed by gently bubbling argon for 10 min and left 5 seconds to equilibrate before measurements.

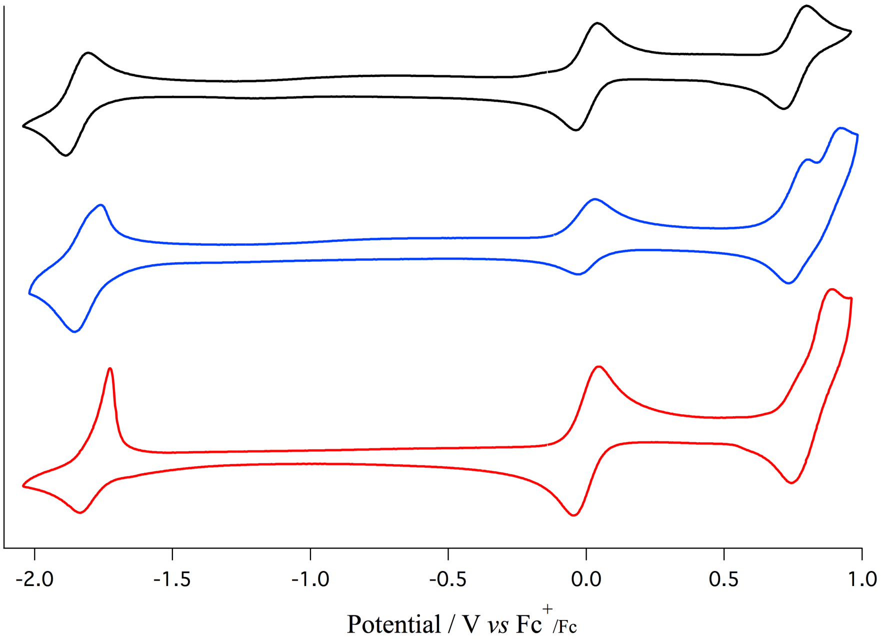

Figure S4. Voltammograms of **Ir0** (black, top), **Ir1** (blue (middle) and **Ir2** (red, bottom). The signal at 0 V is for the ferrocene.

IV. Spectroscopy

Steady state absorption and photoluminescence measurements

All absorption spectra recorded in this work were recorded on a Cary 5G UV-Vis-NIR (Varian) spectrophotometer using 10, 2 and 1 mm synthetic quartz (Suprasil) cells. Fluorescence quantum yield studies of degassed solutions were performed using a Fluorolog-3 (Jobin Yvon) spectrofluorometer with iHR-320 and photomultipliers from Hamamatsu Photonics: R2658 (range 280–1100 nm) with reference $[Ru(bpy)_3]^{2+}$ in water ($\Phi_{fl} = 0.028$).

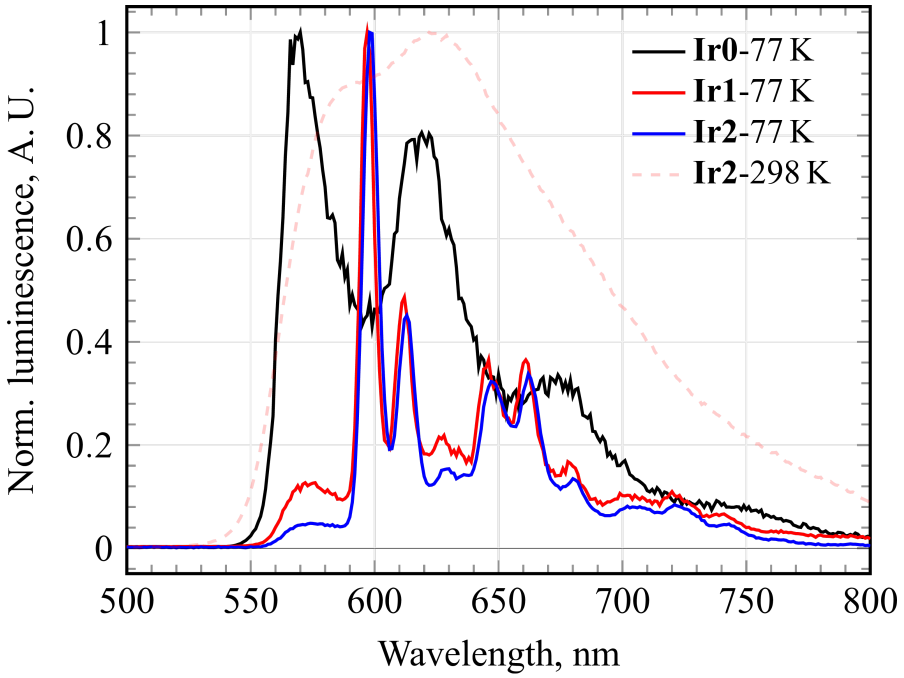

Figure S5. Steady-state luminescence of **Ir0**, **Ir1** and **Ir2** at 77 K (dot-dashed line) in butyronitrile (λ_{exc} = 413 nm).

Time-resolved measurements

The sub-nanosecond transient absorption / time-resolved luminescence set-up was built as follows (Figure S6): a frequency tripled Nd:YAG amplified laser system (30 ps, 30 mJ @1064 nm, 20 Hz, Ekspla model PL 2143) output was used to pump an optical parametric generator (Ekspla model PG 401) producing tunable excitation pulses in the range 410 – 2300 nm. The residual fundamental laser radiation was focused in a high pressure Xe filled breakdown cell where a white light pulse for sample probing was produced. For longer scales (micro- and milliseconds), the white light probe was obtained using an ensemble of light emitting diodes (Roithner Lasertechnik, from 365 to 710 nm) working in flash mode in a multi-furcated fiberoptic cable (8-cores, Avantes) All light signals were analysed by a spectrograph (Princeton Instruments Acton model SP2300) coupled with a high dynamic range streak camera (Hamamatsu C7700, 1ns-1ms). Accumulated sequences (sample emission, probe without and with excitation) of pulses were recorded and treated by HPDTA

(Hamamatsu) software to produce two-dimensional maps (wavelength *vs* delay) of transient absorption intensity in the range 300 – 800 nm. Typical measurement error was better than 10^{-3} O. D. Data were analysed using home-made software developed in LabVIEW 2014 system-design platform and development environment. The trust-region dogleg algorithm[3] (supported by LabVIEW 2014) was applied to determine the set of parameters that best fit the set of input data. The trust-region dogleg algorithm was used instead of Levenberg-Marquardt algorithm, the latter being less stable in most cases during optimization process, because trust region methods are robust, and can be applied to ill-conditioned problems. The emission lifetimes were also verified by measurements using a MultiChannel Scaling (MSC) technique. A Piccolo-AOT MOPA Nd:YVO (Innolas lasers, Germany) variable frequency (10 − 5000 Hz) laser with 800 ps pulses was used to generate the third harmonic, 355 nm, which was used as an excitation source.

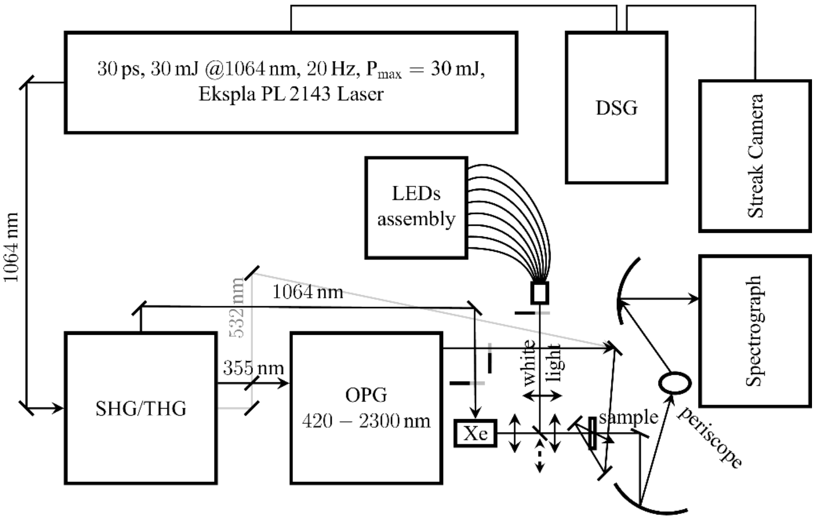

Figure S6. Scheme for sub-nanosecond laser set-up; SHG/THG – second/third harmonic generator, OPG – optical parametric generator, LED – light emitting diode, DSG – digital signal generator.

The fast counting card P7879 100ps/10GHz Time off flag/Multiscaler (Comtex GmBH, Germany) was triggered by every laser pulse event generation (1000 Hz) in order to count photons detected by detector. The excitation and detection system were set to produce 10000cps, which were distributed over 1200 bins (208 ns/bin, overall >2.5 ms).

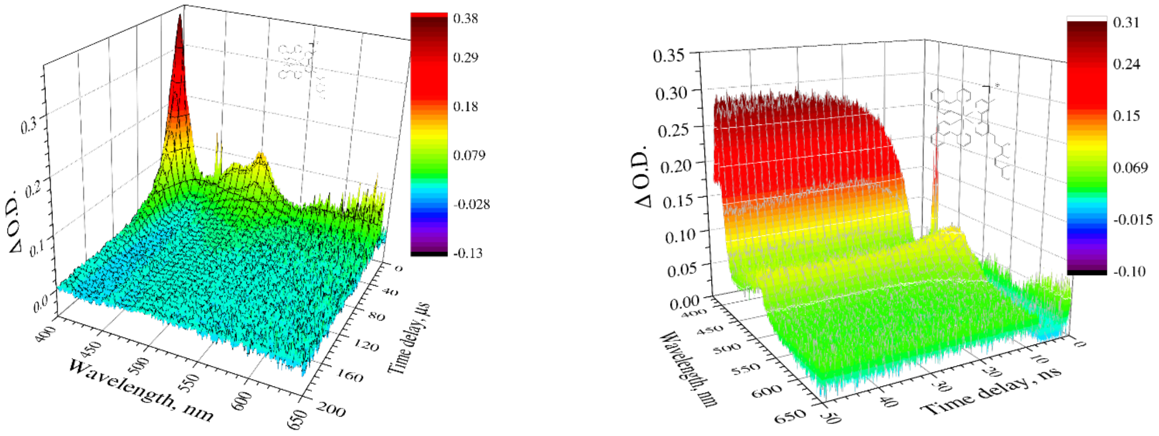

Figure S7. Transient absorption map of **Ir1** on different timescales in acetonitrile at room temperature (λ_{ex} = 430 nm, 186 μM), showing (a) real time energy distribution leading to equilibration between ^{3}MLCT and ^{3}Pyr excited states, b) deexcitation of the equilibrated bichromophoric molecule.

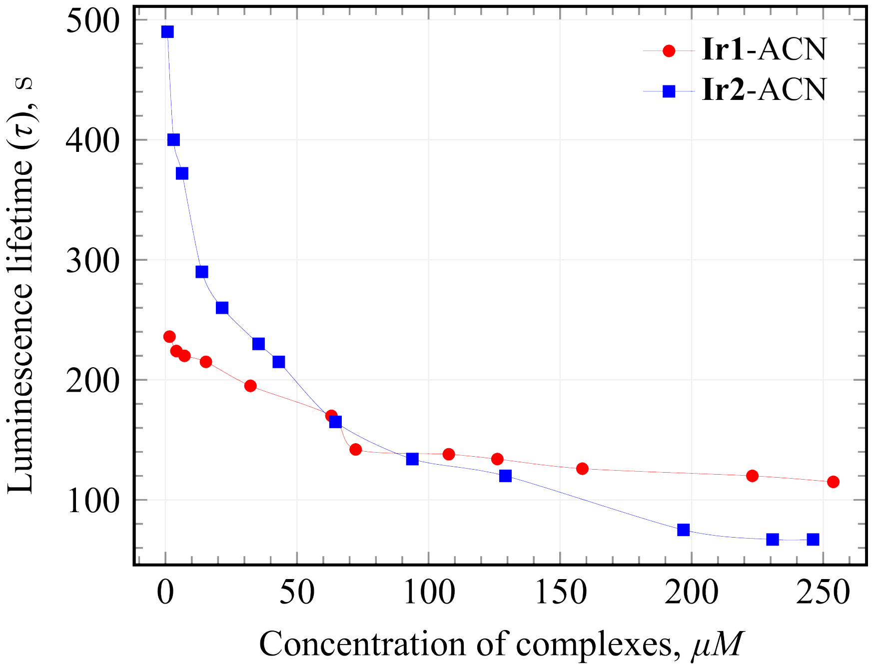

Figure S8. Concentration dependence of luminescence lifetime of **Ir1** and **Ir2** in acetonitrile.

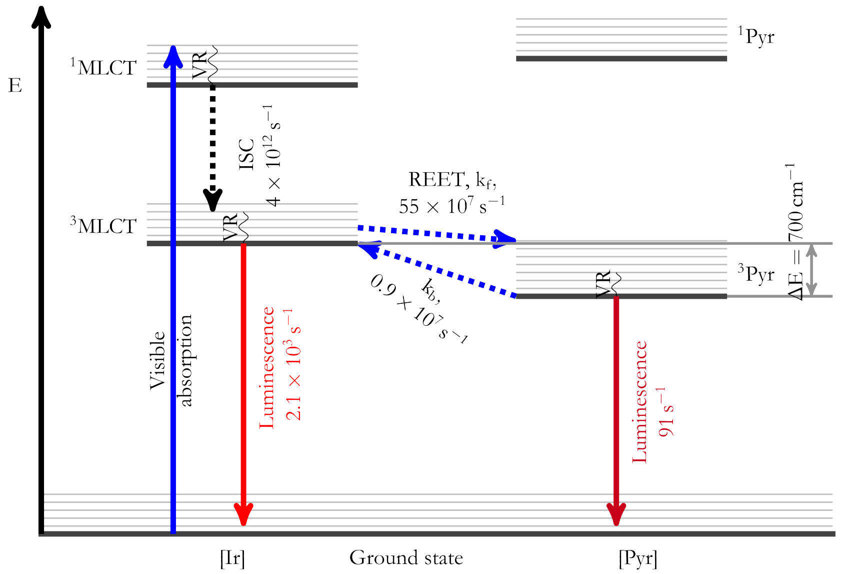

Figure S9. Jablonski diagram showing pertinent energy levels and kinetics of interchromophore energy transfer and luminescence of **Ir2**. VR = vibrational relaxation, ISC = Intersystem crossing, REET = Reversible electronic energy transfer.

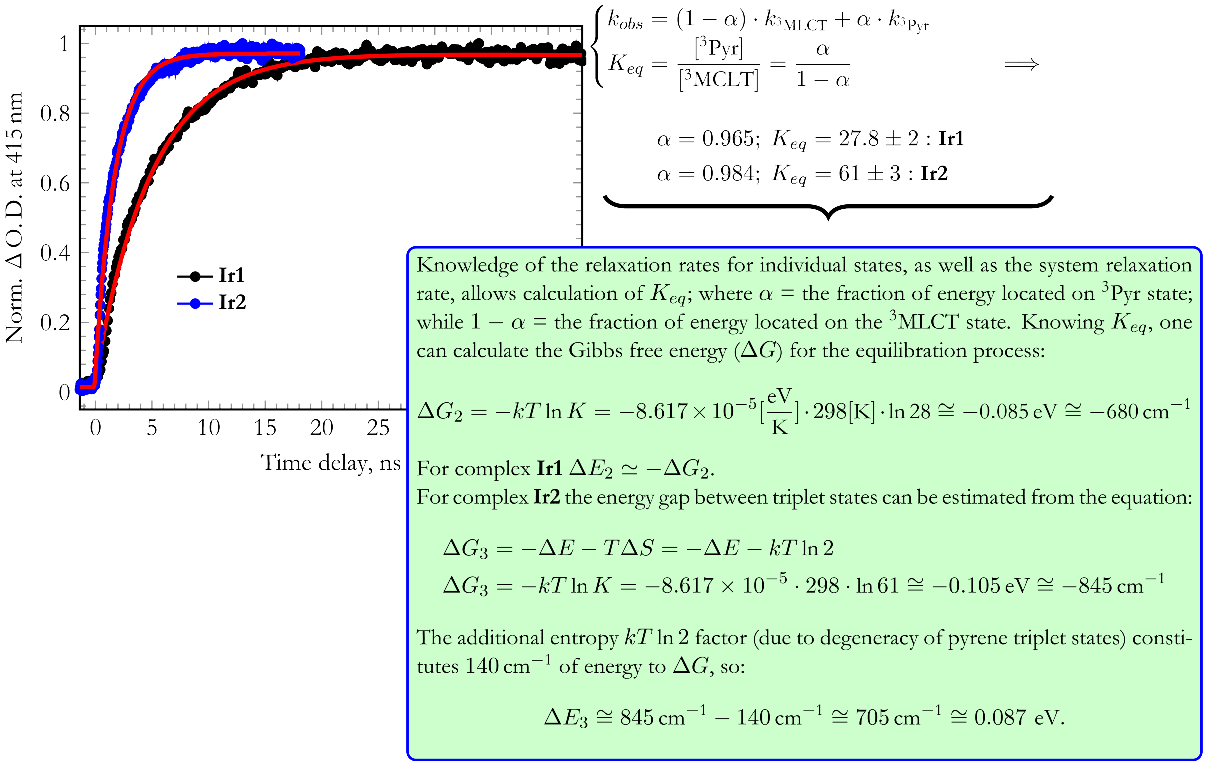

$$\begin{cases} k_{obs} = (1-\alpha)\cdot k_{^3\mathrm{MLCT}} + \alpha\cdot k_{^3\mathrm{Pyr}} \\ K_{eq} = \dfrac{[^3\mathrm{Pyr}]}{[^3\mathrm{MCLT}]} = \dfrac{\alpha}{1-\alpha} \end{cases} \Longrightarrow$$

$$\alpha = 0.965;\ K_{eq} = 27.8 \pm 2 : \mathbf{Ir1}$$

$$\alpha = 0.984;\ K_{eq} = 61 \pm 3 : \mathbf{Ir2}$$

Knowledge of the relaxation rates for individual states, as well as the system relaxation rate, allows calculation of K_{eq}; where α = the fraction of energy located on ^{3}Pyr state; while $1-\alpha$ = the fraction of energy located on the ^{3}MLCT state. Knowing K_{eq}, one can calculate the Gibbs free energy (ΔG) for the equilibration process:

$$\Delta G_2 = -kT\ln K = -8.617\times 10^{-5}[\frac{\mathrm{eV}}{\mathrm{K}}]\cdot 298[\mathrm{K}]\cdot \ln 28 \cong -0.085\ \mathrm{eV} \cong -680\ \mathrm{cm}^{-1}$$

For complex **Ir1** $\Delta E_2 \simeq -\Delta G_2$.
For complex **Ir2** the energy gap between triplet states can be estimated from the equation:

$$\Delta G_3 = -\Delta E - T\Delta S = -\Delta E - kT\ln 2$$
$$\Delta G_3 = -kT\ln K = -8.617\times 10^{-5}\cdot 298\cdot \ln 61 \cong -0.105\ \mathrm{eV} \cong -845\ \mathrm{cm}^{-1}$$

The additional entropy $kT\ln 2$ factor (due to degeneracy of pyrene triplet states) constitutes 140 cm^{-1} of energy to ΔG, so:

$$\Delta E_3 \cong 845\ \mathrm{cm}^{-1} - 140\ \mathrm{cm}^{-1} \cong 705\ \mathrm{cm}^{-1} \cong 0.087\ \mathrm{eV}.$$

Figure S10. Method for determination of energy gap between ^{3}MLCT and ^{3}Pyr states (green box). Approach to excited-state equilibrium following excitation monitored by growth of ^{3}Pyr transient absorption signature at 415 nm (top left).

V. Oxygen sensing

Preparation and characterization of the oxygen-sensing films.

Polystyrene (PS) was obtained from Scientific Polymers, and AP200/19 metal oxide support was prepared by Ilford Imaging Switzerland following the procedure previously published.[4-6] Nitrogen and oxygen (all of 99.999% purity) were obtained from Air Liquide.

The cocktails were prepared by dissolving the dyes into 2 mL of chloroform (dye concentration of 1.5 mg mL^{-1}). In the case of polystyrene films, 200 mg of the polymer (PS) were added to each cocktail. The cocktails were shaken on an IKA-Vibramax-VXR (IKA-Labortechnik, Staufen, Germany) until the dye was completely dissolved. The oxygen-sensitive membranes were obtained using a Laurell spin-coater (WS-400B-6NPP/LITE, Laurell Technologies). For the AP200/19 membranes, 100 µL of the cocktail were injected onto the rotating metal oxide support fixed onto a spinning device at 300 rpm. For the PS membranes, 300 µL of the cocktail were injected onto the rotating glass support fixed onto a spinning device at 700 rpm. All membranes obtained were translucent, allowing some visible light to pass through them. Three replicas were prepared for each membrane to evaluate the error. All the experimental results were expressed as the average of 3 replicas ± error ($s\cdot t/\sqrt{n}$), where *s* is the standard deviation, *t* is the Student's t, and *n* is the number of replicas.

The control of oxygen was carried out with a gas-station developed at our laboratories based on two mass flow controllers (MFC) of Type EL-FLOW® model F-201CV Bronkhorst High-Tech. Copper and stainless steel tubing was used to connect the MFCs with the self-built flow-through cell as previously reported.[7] This gas-station was controlled by a LabView 8.2 program connected to a Flow Bus interface (Bronkhorst) that completely controls the Bronkhorst mass-flow controllers *via* RS-232.

Excitation and emission spectra as well as intensity measurements were acquired on a Varian Cary-Eclipse luminescence spectrometer (Varian Inc.-Agilent Technologies) exciting the sensing films at 344 nm and recording the luminescent emission at 582 nm with a detector voltage of 530 and 550 v for PS and AP200/19 sensing films and 10 nm excitation and emission slit widths. Lifetime measurements were carried out with the multifrequency measurement system developed by our research group;[8, 9] a short description of this equipment is given below.

All measurements were performed at room temperature (21 ºC). The temperature was continuously monitored using a commercial temperature sensor (MicroLite, Fourtec-Fourier Technologies).

A standard protocol was used for characterizing the membranes.[8] To obtain the Stern-Volmer Plot (SVP), the oxygen partial pressures were calculated from the measured oxygen/nitrogen flows, assuming a constant environmental pressure of 100 kPa. Intensity and lifetime measurements were made at 14 different oxygen partial pressures between 0-10 kPa and 0-1 kPa. To demonstrate the sensitivity for ultra-low oxygen detection, the gas station was modified by replacing the pure oxygen with synthetic air (mixture of oxygen and nitrogen) to achieve a minimum oxygen concentration of 0.05 kPa pO_2.

Luminescence quenching methods are based on the decrease in luminescence intensity or lifetime in the presence of the quencher (oxygen), and they are described by the Stern-Volmer equation:[10, 11]

$$\frac{I_0}{I} = \frac{\tau_0}{\tau} = \left[\sum_{i=1}^{n} \frac{x_i}{1 + K_{SV,i} \cdot pO_2} \right]^{-1}$$

where I is the luminescence intensity, τ is the luminescence lifetime, n is the number of microdomains, the subindex 0 represents unquenched conditions, and x_i denotes the fractional contribution of the total luminescence emission from the luminophore located at site type i, which exhibits a discrete Stern-Volmer quenching constant given by $K_{SV,i}$.

The apparent luminescence lifetimes were determined by phase-resolved luminescence[11] using a multifrequency phase-modulation method that uses rectangular-wave signals with a short duty cycle to modulate the excitation light source.[8] The use of short duty-cycle rectangular signals for excitation provides several harmonics with enough amplitude for allowing the simultaneous measurement of phase shift and modulation factor at several frequencies.

Short description of the instrument used for lifetime measurements

An ultraviolet LED was used as light source (Ocean Optics, LED-375, λ_{max} = 375 nm, angle of illumination 15º, LED diameter 5 mm, luminous power 25 µW) filtered through an optical band-pass filter (Thorlabs GmbH, MF390-18, $\lambda_{central}$ = 390 nm). This LED is modulated by a rectangular-wave signal with 10% duty cycle at appropriate modulation frequency. The excitation signal is numerically generated with a computer and is provided by the analog output channel on an AD/DA board (NI PCIe-6363/ BNC-2120, National Instruments, USA) at a sampling rate of 500 kS/s. This excitation signal is applied to the LED driving circuit in order to modulate the current in the LED. The voltage in a resistor in series with the LED is used as reference excitation signal. The emission signal is transduced with a photomultiplier tube (PMT) with a bandwidth dc-1 MHz (H10723-20, Hamamatsu Photonics, Japan) equipped with an appropriate optical band-pass filter, and the PMT output is amplified and filtered with appropriate analogue electronics. Both the excitation signal (the reference) and the emission signal from the sensing film are simultaneously digitized *via* a digital oscilloscope WaveRunner 604Zi (LeCroy, USA) at 500 kS/s using signals of 1 s in duration (i.e., a 500 kS data buffer). The bandwidth of the electronic devices and the sampling rates are large enough for the frequency of the harmonics involved in these experiments and they are also appropriate for the typical lifetimes of the used complexes (lifetimes in the range of tens of microseconds).

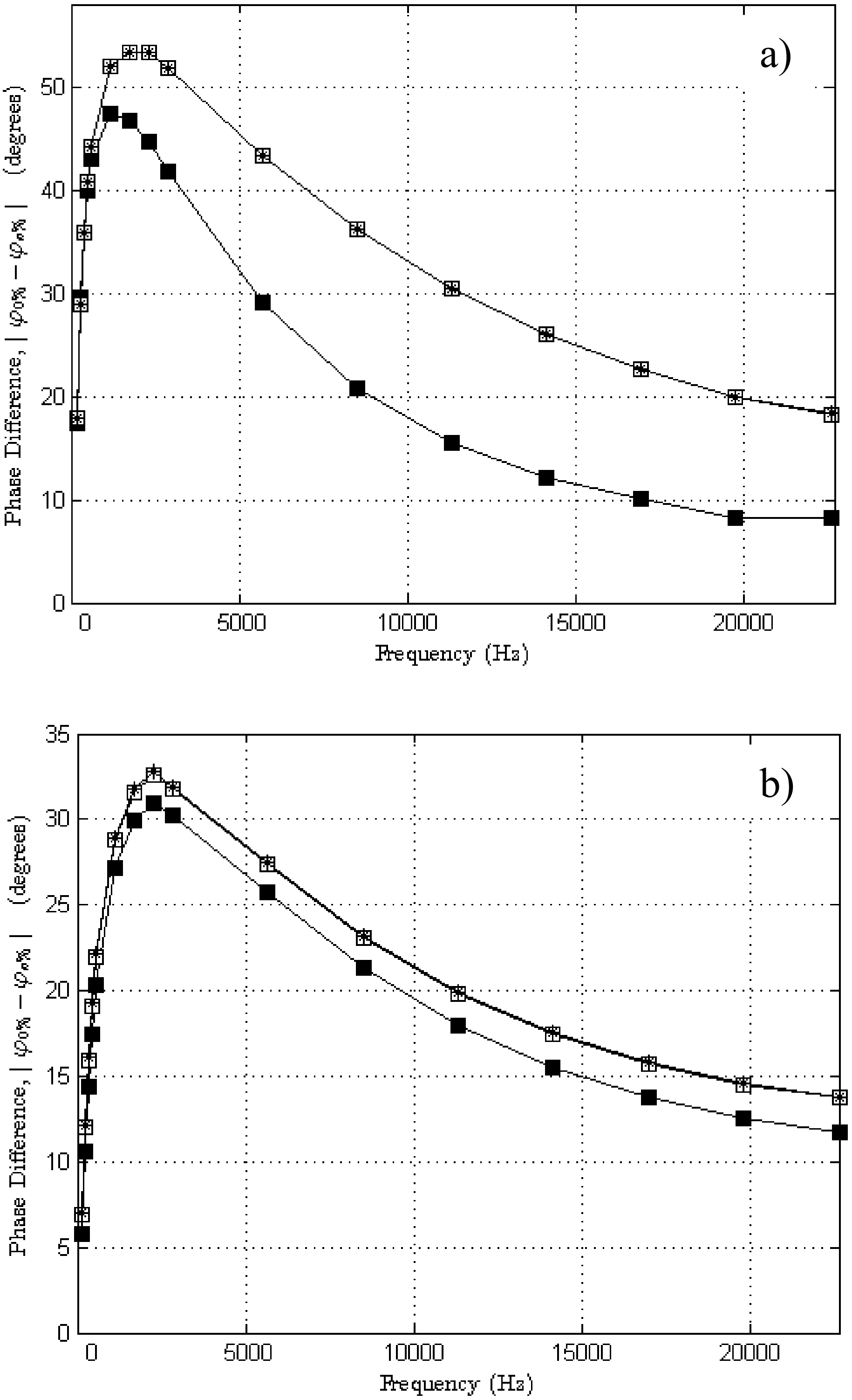

Figure S11. Effect of the modulation frequency on the average phase difference at several oxygen concentrations (■ from 0 to 1 kPa pO_2, □ from 0 to 10 kPa pO_2) of **Ir2** incorporated into a) PS and b) AP200/19 at 21 ºC. Modulation frequencies of 1130 Hz and 2260 Hz were selected for the sensing films **Ir2**-PS and **Ir2**-AP200/19 respectively.

Table S2. Measurement capability of the developed sensing films using luminescence intensity measurements and apparent luminescence lifetime measurements determined from the phase shift. The data are shown in kPa and the relative error (into bracket) in %.

Intensity measurements (I)			Apparent lifetime measurements (τ_{φ})		
Real pO_2, kPa	**Ir2**-PS	**Ir2**-AP200/19	Real pO_2, kPa	**Ir2**-PS	**Ir2**-AP200/19
1.00	0.986 (1.46)	0.974 (2.55)	0.05	0.049 (2.62)	0.051 (2.51)
2.00	1.963 (1.87)	2.143 (7.08)	0.21	0.215 (2.19)	0.218 (3.96)
3.00	2.943 (1.92)	3.232 (7.73)	1.05	1.067 (1.62)	1.033 (2.05)
4.00	3.942 (1.57)	4.082 (2.93)	1.47	1.504 (2.15)	1.428 (2.89)
5.00	4.926 (1.64)	4.773 (4.57)	2.10	1.986 (5.54)	2.161 (3.18)
7.00	6.781 (3.17)	6.372 (8.97)	4.00	3.830 (4.92)	4.115 (3.46)

[a] All values correspond to the average of 50 measurements. Calibration curves obtained for the luminescence intensity measurements (I, expressed in arb. units) in the range of 0-10 kPa pO_2 were used.

[b] All values correspond to the average of 50 measurements. Calibration curves obtained for the apparent lifetimes determined from the phase-shift (τ_{φ}, expressed in microseconds) at a single modulation frequency in the range of 0-10 kPa pO_2 were used.

VI. References

1. S. A. Denisov, Y. Cudre, P. Verwilst, G. Jonusauskas, M. Marin-Suarez, J. F. Fernandez-Sanchez, E. Baranoff and N. D. McClenaghan, *Inorg. Chem.*, 2014, **53**, 2677.
2. N. D. McClenaghan, F. Barigelletti, B. Maubert and S. Campagna, *Chem. Commun.*, 2002, 602.
3. M. L. A. Lourakis and A. A. Argyros, *Computer Vision, 2005. ICCV 2005. Tenth IEEE International Conference on*, 2005, **2**, 1526.
4. J. F. Fernández-Sánchez, R. Cannas, S. Spichiger, R. Steiger and U. E. Spichiger-Keller, *Anal. Chim. Acta*, 2006, **566**, 271.
5. J. F. Fernández-Sánchez, I. Fernández, R. Steiger, R. Beer, R. Cannas and U. E. Spichiger-Keller, *Adv. Funct. Mater.*, 2007, **17**, 1188.
6. M. Marín-Suárez del Toro, J. F. Fernández-Sánchez, E. Baranoff, M. K. Nazeeruddin, M. Gräetzel and A. Fernández-Gutiérrez, *Talanta*, 2010, **82**, 620.
7. A. L. Medina-Castillo, J. F. Fernández-Sánchez, C. Klein, M. K. Nazeeruddin, A. Segura-Carretero, A. Fernández-Gutiérrez, M. Graetzel and U. E. Spichiger-Keller, *Analyst*, 2007, **132**, 929.
8. S. Medina-Rodríguez, A. de la Torre-Vega, F. J. Sainz-Gonzalo, M. Marín-Suárez, C. Elosúa, F. J. Arregui, I. R. Matias, J. F. Fernández-Sánchez and A. Fernández-Gutiérrez, *Anal. Chem.*, 2014, **86**, 5245.
9. P. J. R. Roche, M. C. K. Cheung, K. Y. Yung, A. G. Kirk, V. P. Chodavarpu and F. V. Bright, *Sens. Act. B*, 2010, **147**, 581.
10. J. N. Demas and B. A. DeGraff, *Sens. Act. B*, 1993, **11**, 35.
11. J. R. Lakowicz, *Principles of Fluorescence Spectroscopy*, Kluwer Academic, New York, 2nd edn., 1999.